



Cite this: *RSC Adv.*, 2022, **12**, 3924

Received 17th December 2021
 Accepted 18th January 2022

DOI: 10.1039/d1ra09128j

rsc.li/rsc-advances

1. Introduction

Perovskites have been widely applied in solar cells,^{1–4} light-emitting diodes,^{5–7} photodetectors^{8–10} and lasers¹¹ due to their facile solution-processability, long carrier diffusion length and high carrier mobility.¹² Recently, flexible optoelectronic devices have attracted intensive interest because of their promising applications in wearable devices, biosensors and smart textiles. To fabricate flexible optoelectronic devices, all photosensitive materials, electrodes and substrates must be optimized to meet the requirements of flexibility, light weight, low cost and stability.^{13–15} To date, diverse plastic substrates, such as polyethylene terephthalate (PET) and poly(ethylene naphthalate) (PEN), are used to fabricate flexible perovskite optoelectronic devices.^{16–19} Li and co-workers demonstrated a solution method to fabricate photodetector on a PET substrate, which displayed a high on/off ratio and responsivity.²⁰ Li *et al.* reported a flexible photodetector on ITO/PEN substrate with outstanding stability and satisfactory detectivity.²¹ However, low thermal durability and high thermal expansion coefficient of plastics always obstruct the manufacturing processes. More importantly, plastic substrates are difficult to degrade in nature.

Paper is usually made of natural cellulose fibers, it can be degraded completely in 6 weeks.^{22,23} Recently, paper is

Pen-writing high-quality perovskite films and degradable optoelectronic devices†

Ting Zhang,^a Shasha Zhang,^a Zhenkun Gu,^{*a} Rudai Zhao,^a Shiheng Wang,^a Lutong Guo,^{bc} Tiesheng Li,^{id}^a Yiqiang Zhang^{id}^a and Yanlin Song^{id}^{*bc}

Paper is ubiquitous in the daily life and has been widely used for writing and drawing because of their low-cost, widely accessible, and degradable properties. However, simple ways to fabricate paper-based optoelectronic devices remain a great challenge. In this work, we report a facile method to fabricate high-quality perovskite films and optoelectronic devices on paper by direct pen-writing. Through introducing seed layers on papers, planar-integrated single-crystal perovskite films are easily prepared using commercial pens. Based on such a simple and convenient method, perovskite photodetector arrays and image sensors with graphite electrodes are fabricated on paper, and show satisfactory performances. This method provides a simple and effective approach for preparation of paper-based perovskite devices. It will be of significance for the development of degradable optoelectronic devices.

considered as a promising substrate material for flexible electronics because of its lightweight, deformability, and biodegradability, which accords with the development trend of modern electronic products towards flexible devices.^{22,24} Chu *et al.* reported a dual-source physical vapor deposition processed photodetector on cellulose paper substrates with high photo detecting performance.²⁵ Yang and coworkers prepared the flexible photodetector arrays on common paper by an all-sprayed-processable method.²⁶ However, these traditional methods are complicated and time-consuming. More importantly, the perovskite crystals by these methods have poor quality. Therefore, the development of a facile approach to fabricate paper-based perovskite optoelectronic devices is of significance.^{27–29}

Herein, we report a facile method to construct high-quality perovskite films and devices on paper by pen-writing. Through introducing the seed layers on paper, planar-integrated single-crystal perovskite films are prepared by commercial pens. Using perovskite material and graphite as the photosensitive layer and electrode, large-scale photodetector arrays are easily written on paper. The photodetector presents a responsivity of 4.2 mA W^{−1} at a low operational bias voltage of 4 V. Furthermore, an image sensor is fabricated, which shows satisfied performance. This method provides a simple and effective strategy for the development of paper-based optoelectronic devices.

2. Experimental section

2.1 Material

Methylammonium bromide (CH₃NH₃Br; ≥99.5%) was purchased from Xi'an Polymer Light Technology Corp. Lead bromide (PbBr₂; 99.999%) and *N,N*-dimethylformamide (DMF,

^aGreen Catalysis Center, College of Chemistry, Henan Institute of Advanced Technology, Zhengzhou University, Zhengzhou 450051, China. E-mail: guzhenkun@zzu.edu.cn

^bKey Laboratory of Green Printing, Institute of Chemistry, Chinese Academy of Sciences, Beijing 100190, China. E-mail: ylsong@iccas.ac.cn

^cUniversity of Chinese Academy of Sciences, Beijing 100049, China

† Electronic supplementary information (ESI) available: Fig. S1–S7, Table S1–S2 and Movie S1. See DOI: 10.1039/d1ra09128j



$\geq 99.9\%$) were purchased from Aladdin Reagent Ltd. The weighing paper was purchased from Wuxi Shangrui Paper Co., Ltd. The office-copy paper was purchased from Yalong Paper Products (Kunshan) Co., Ltd. The filter paper was purchased from Hangzhou Special Paper Co., Ltd. All these materials were used as received without further purification.

2.2 Preparation of $\text{CH}_3\text{NH}_3\text{PbBr}_3$ solution

PbBr_2 and $\text{CH}_3\text{NH}_3\text{Br}$ were dissolved in DMF and stirred at 60°C for 6 h to prepare the 0.5 mol L^{-1} $\text{CH}_3\text{NH}_3\text{PbBr}_3$ solution.

2.3 Preparation of perovskite films by pen-writing

0.5 mol L^{-1} $\text{CH}_3\text{NH}_3\text{PbBr}_3$ -DMF was written on paper by a commercial pen (Geemarker, Hong Kong, China) with controlled speed and temperature.

2.4 Spin-coating

Before spin-coating, the weighing paper was treated with UV-ozone for 15 min. 0.5 mol L^{-1} $\text{CH}_3\text{NH}_3\text{PbBr}_3$ -DMF was spin-coated on the paper at 1000 rpm for 30 s and then annealed at 80°C for 5 min in ambient air. The film was cooled to room temperature, and the spin-coating was continued under the same conditions for 5 times.

2.5 Device fabrication

Graphite-pencil (9B) drawing guided by ruler and masks was repeated 20 times to form a stripe of uniform electrode on office-copy paper. The left and right pencil-traces were both 2 mm wide and 50 mm long. The spacing between adjacent electrodes was about 300 μm . Filled the ink into the pen, and fixed the pen on a dispenser (Nordson) for writing. Placed the paper on a hot plate at 80°C , and chose an appropriate speed to write on the paper. After solvent evaporation, the photodetector was obtained.

2.6 Characterization

The crystals were examined by X-ray diffraction (XRD) with $\text{Cu K}\alpha$ radiation (Empyrean, Holland). Optical images of perovskite single-crystal films were obtained using a Nikon LV100ND optical microscope. Scanning electron microscopy (SEM) image was measured by JEOL JSM-7500F (Japan). Transmission electron microscopy (TEM) images were characterized by JEOL JEM-1011 (Japan). The absorption was performed by ultraviolet-visible (UV-vis) spectrophotometer (Shimadzu UV 2600). The photoluminescence (PL) was measured with the wavelength ranging from 510 to 650 nm at room temperature by a fluorescence spectrophotometer (Horiba FluoroMax+). Time-resolved

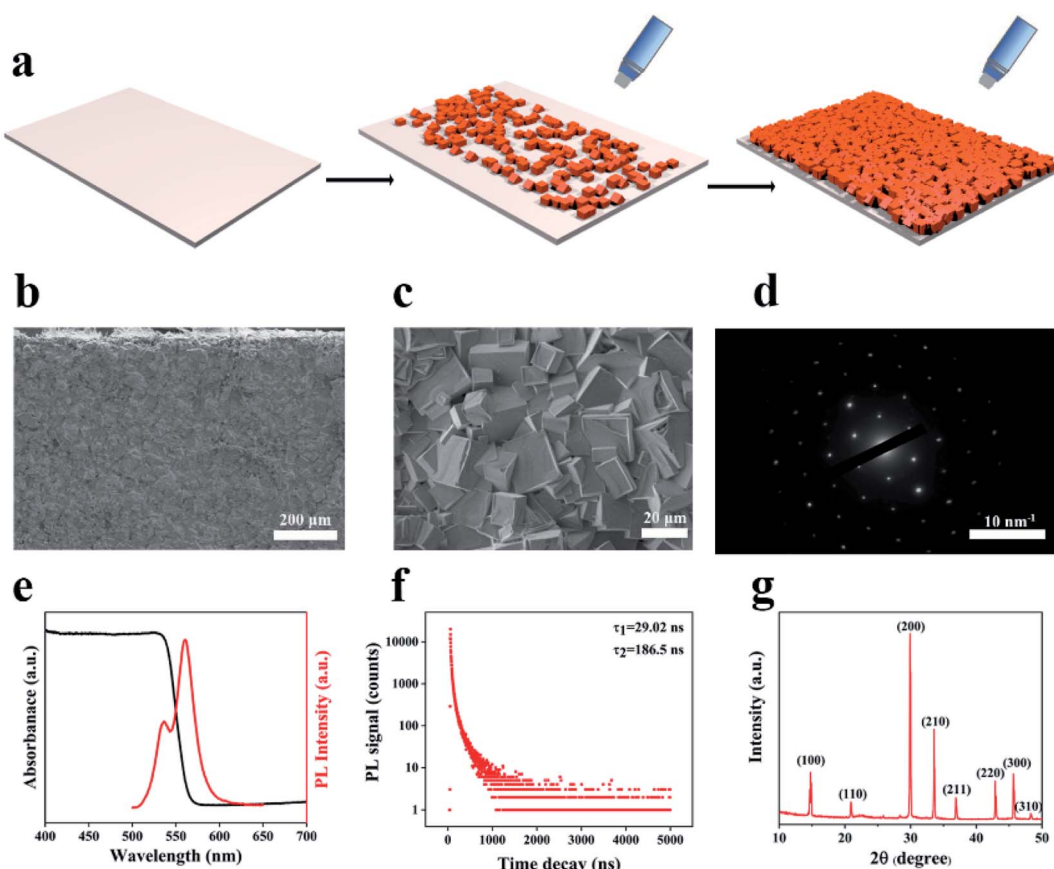


Fig. 1 (a) Schematic illustration of pen-writing perovskite films. (b and c) SEM images of the pen-writing $\text{CH}_3\text{NH}_3\text{PbBr}_3$ films. (d) TEM of individual grain of $\text{CH}_3\text{NH}_3\text{PbBr}_3$ films. (e) Visible absorption and PL spectra of the prepared $\text{CH}_3\text{NH}_3\text{PbBr}_3$ films. (f) PL time decay trace of the $\text{CH}_3\text{NH}_3\text{PbBr}_3$ films. (g) XRD data of the $\text{CH}_3\text{NH}_3\text{PbBr}_3$ films.



photoluminescence (TRPL) spectrum was tested using an Edinburgh Instruments FS980 system. The current–voltage (*I*–*V*) traces were measured using a Micromanipulator probe station with a Keithley 4200 semiconductor measurement system at room temperature.

3. Results and discussion

Fig. 1a shows the schematic illustration of the preparation of perovskite films by pen-writing. First, perovskite solution was written on paper to form a perovskite seed layer. Then, perovskite ink was written on the seed layer for several times, and a planar-integrated single-crystal perovskite film was obtained. The morphology of pen-writing perovskite films is shown in Fig. 1b and c. It reveals that the paper substrate is covered with a dense perovskite film. In the film, the crystals are connected to each other well, forming a laterally continuous planar-integrated single-crystal perovskite structure.^{30,31} To further

confirm the high structural order of the planar-integrated single-crystal perovskite films, transmission electron microscopy (TEM) was performed (Fig. 1d). The well-defined Bragg reflection in symmetric TEM pattern confirms the single crystal structure of the integrated crystals.³² Fig. 1g presents the X-ray diffraction (XRD) of the $\text{CH}_3\text{NH}_3\text{PbBr}_3$ film. It shows a set of diffraction peaks at 14.83° , 20.92° , 29.92° , 33.57° , 37.06° , 42.98° , 45.75° and 48.34° , corresponding to the (100), (110), (200), (210), (211), (220), (300) and (310) planes of the $\text{CH}_3\text{NH}_3\text{PbBr}_3$ crystal, respectively.³³ The sharp diffraction peaks demonstrate the perovskite structure with high purity.

To investigate the quality of the perovskite film, the visible absorption and photoluminescence (PL) spectra were characterized. The absorption profile shows that the band edge is located at 571 nm, while the PL peak position of $\text{CH}_3\text{NH}_3\text{PbBr}_3$ film is located at 560 nm (Fig. 1e). This low Stokes shift indicates a small vibronic relaxation.³⁰ Compared with the spin-coated film (Fig. S1†), the steep rise at the band edge in the

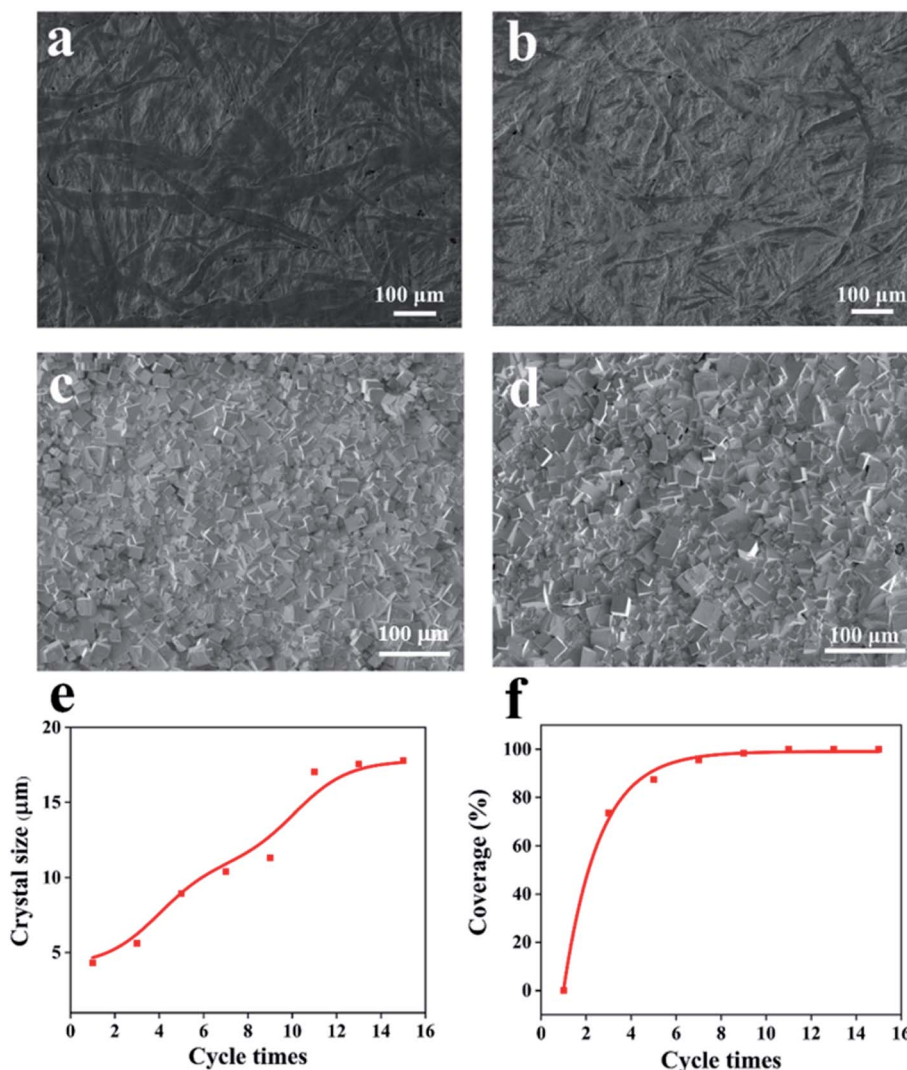


Fig. 2 (a–d) SEM images of the $\text{CH}_3\text{NH}_3\text{PbBr}_3$ films prepared on paper with different writing cycles. (a) 1 times, (b) 5 times, (c) 10 times, (d) 15 times. (e) The sizes of crystals as a function of writing times. (f) The coverage of films as a function of writing times.



absorption spectrum suggests a low concentration of in-gap defects.^{30,34} The PL emission peak presents a red shift, which is closer to the PL emission peak of the bulk crystal, indicating that the films prepared by this method have a high crystal quality.^{35,36} Moreover, the narrow full width at half maximum (FWHM) of the PL spectrum also indicates that the film has low defects. PL decay has been widely used as a figure of merit for carrier recombination. It shows a fast and a slow time constant of $\tau_1 \sim 29.02$ ns and $\tau_2 \sim 186.5$ ns (Fig. 1f), which are associated with surface and bulk recombination, respectively. The charge carrier lifetimes of the pen-writing perovskite film ($\tau_1 \sim 29.02$ ns and $\tau_2 \sim 186.5$ ns) are much longer than the spin-coated film ($\tau'_1 \sim 3.7$ ns and $\tau'_2 \sim 14.83$ ns), indicating a lower trap density of the pen-writing film (Fig. S2†).

The scanning electron microscopy (SEM) images of $\text{CH}_3\text{NH}_3\text{PbBr}_3$ films of different writing times are shown in Fig. 2a-d. When the writing times are less than 5, there is less crystal on the paper and the crystal size is small, with an average size below 10 μm (Fig. 2a and b). With the increase of writing cycles, the crystal size and crystal coverage are gradually increasing. When the writing times are 10, the crystals almost completely

cover the paper, while there are still a few holes on the surface (Fig. 2c). With the increase of writing times, the crystal size increases obviously and the film surface becomes denser (Fig. 2d). Finally, an integrated single-crystal perovskite film was prepared.

It suggests that the writing times have a great influence on the formation of integrated single-crystal perovskite films. We investigated the crystallization process of the pen-writing perovskite films (Fig. S3†). It showed that when the writing finished for the first time, the evaporation of solvent has not been completed due to the fast-writing speed (Movie S1†). After the evaporation of solvent, a perovskite seed layer was formed because of the low nucleation barrier caused by the roughness of paper surface. With the writing times increase, fresh perovskite solution is continuously supplied. It was found that the seed crystals were *in situ* grown, eventually forming an integrated single-crystal perovskite film.

Based on this mechanism, planar-integrated single-crystal perovskite films can be effectively prepared on different kinds of paper, including filter paper, office-copy paper and weighing paper (Fig. 3). The corresponding SEM images show that all the

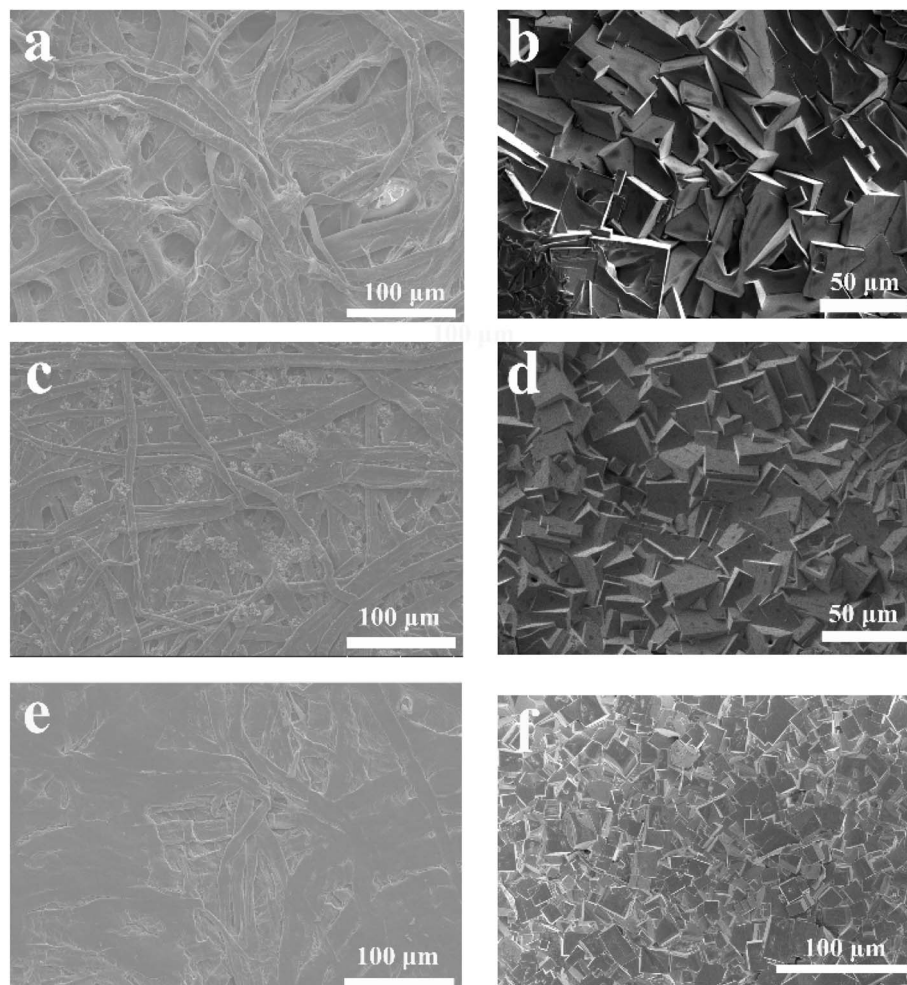


Fig. 3 SEM of the bare paper and $\text{CH}_3\text{NH}_3\text{PbBr}_3$ films. (a) Filter paper. (b) $\text{CH}_3\text{NH}_3\text{PbBr}_3$ film on filter papers. (c) Office-copy paper. (d) $\text{CH}_3\text{NH}_3\text{PbBr}_3$ film on office-copy papers. (e) Weighing paper. (f) $\text{CH}_3\text{NH}_3\text{PbBr}_3$ film on weighing papers.



papers can form satisfied perovskite films by pen-writing. It provides a promising way to construct paper-based perovskite devices.

The pen-writing perovskite films and electrodes enable us to facile prepare photodetector arrays on papers. Fig. 4a and b present the preparation process of the perovskite photodetector by pen-writing. The electrodes with a channel width of 300 μm were constructed on office-copy paper with graphite pencils. Then, perovskite ink was written on electrode channels by a commercial pen to fabricate the perovskite photodetectors. The morphology of the pencil trace was examined by SEM (Fig. 4c). It shows that graphite materials are successfully transferred from the pencil to the paper due to the rough surface of the paper. The layered feature of the graphite flakes can be observed in a magnified view of the sample (Fig. 4d). The resistivity of pencil-drawn electrodes as a function of writing cycles was investigated. The sheet resistivity of the pencil-drawn graphite is inversely correlated with writing cycles, decreasing from $\sim 21.3 \text{ k}\Omega \text{ cm}$ at the first cycle to $\sim 3.62 \text{ k}\Omega \text{ cm}$ at the 20th

cycle (Fig. S5 \dagger). The current–voltage (I – V) characteristics of the photodetector in the dark and under the light illumination (405 nm) with various power intensities are shown in Fig. 4e. It is found that the photocurrent of the photodetector enhances with the increase of the power intensities. Because the photo-generated carriers are separated rapidly by the applied bias voltage, the conductivity of the paper-based perovskite photodetector increases rapidly.³⁷ Fig. S6 \dagger shows the responsivity dependence of the photodetector on the light intensity. At a bias of 4 V, the responsivity decreases from 4.2 mA W^{-1} to 0.22 mA W^{-1} with the increase of input laser power, which is caused by the recombination of electron–hole pairs when irradiated with higher laser intensity.³⁸ With the turn-on and turn-off cycles of the incident laser, the photocurrent accordingly increases to the maximum value (approximately 10^{-6} A) and decreases to the minimum value (approximately 10^{-8} A). The transient photocurrent of the photodetector exhibits satisfied on/off photo switching behavior (Fig. 4f). Fig. S7 \dagger shows the photostability of the device. During the continuous operation of 18 on/off test

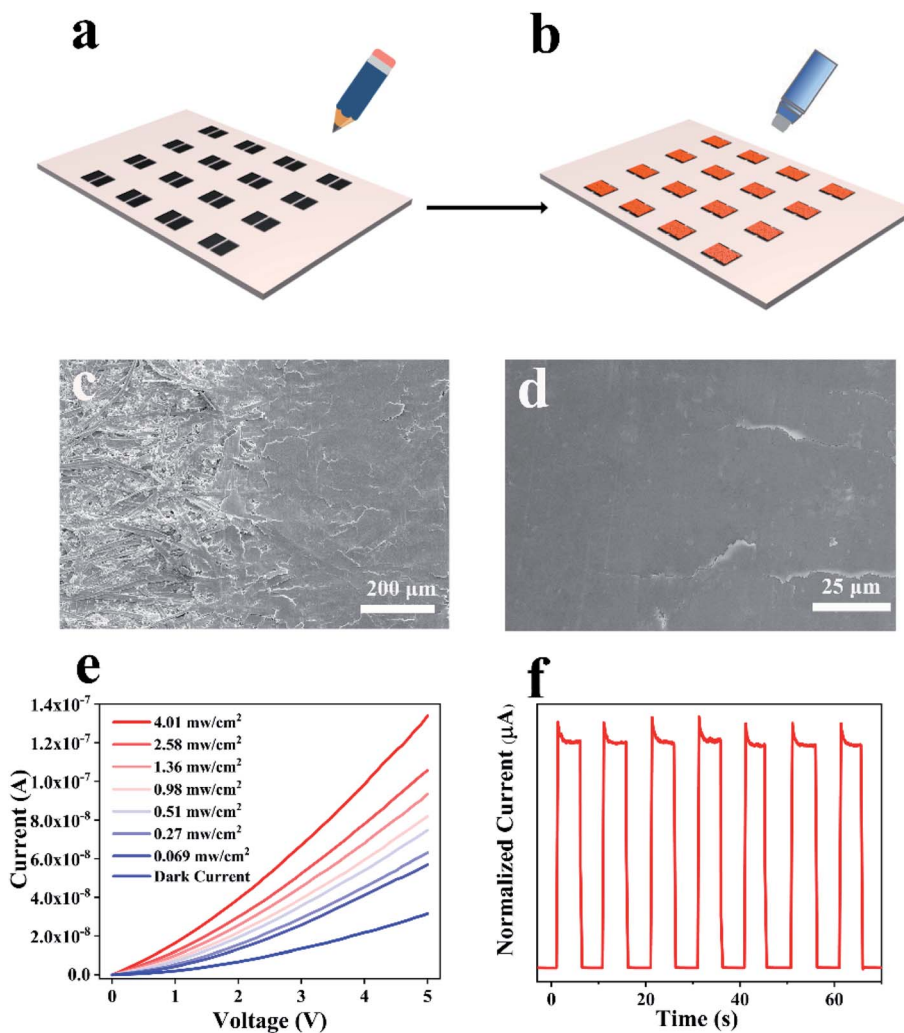


Fig. 4 (a and b) Schematic illustration of the pen-writing photodetectors. (c) SEM image of pencil-drawn graphite on papers. (d) SEM image of the graphitic flakes on papers. (e) I – V curve of the photodetector in different incident light intensities ($\lambda = 405 \text{ nm}$). (f) Transient photocurrent of the photodetector (bias, 3 V; $\lambda = 405 \text{ nm}$).



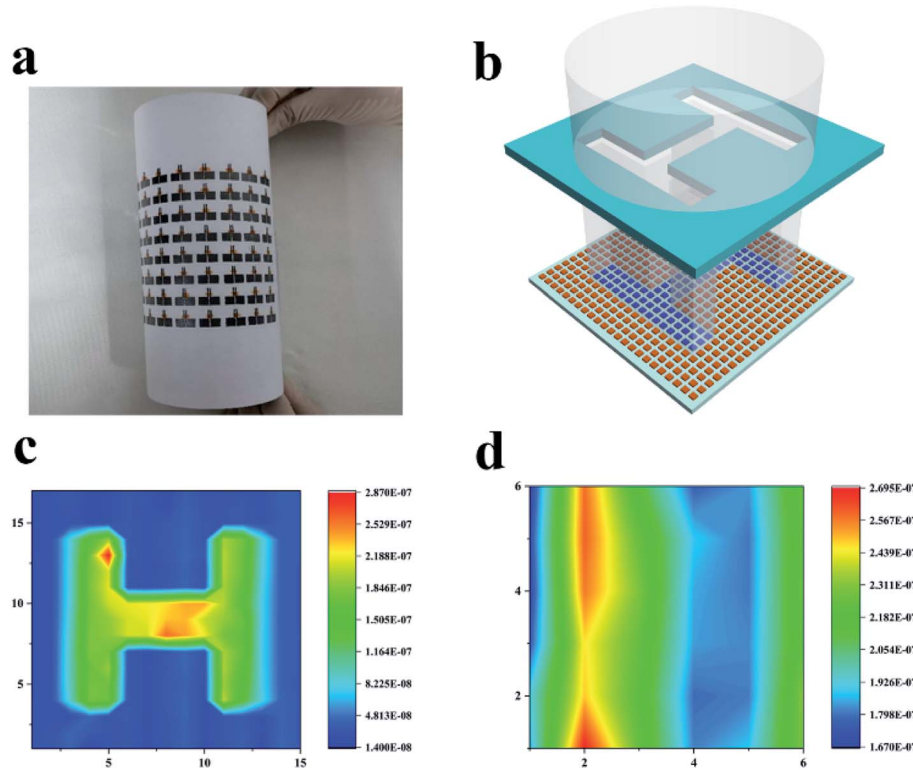


Fig. 5 (a) Photograph of the pen-written perovskite photodetector arrays. (b) Schematic illustration of the image sensor. (c) The characterization of the image sensor (bias, 3 V; $\lambda = 405$ nm). (d) Photocurrent distribution of the photodetector arrays (bias, 3 V; $\lambda = 405$ nm).

cycles, the stable photocurrent shows insignificant degradation. In order to compare the performance of the previously reported perovskite-based photodetector with this work, various device parameters reported in literature are summarized in Table S1.† The performance of the device mainly depends on two aspects: the perovskite film and the electrode. Graphite electrodes fabricated by pencil have a high sheet resistivity ($3.7\text{ k}\Omega\text{ cm}$), result in lower device performance than devices based on gold electrodes.³⁹

Fig. 5a shows a photo of the paper-based photodetector array. An array of 6×6 photodetector was tested. All of them showed obvious photocurrent signals to the light (Fig. 5d). Furthermore, a mask is placed between the pen-writing photodetector arrays and the light source, a patterned letter "H" is transmitted to realize photo-communication (Fig. 5b). Through the photoelectric performance test of these photodetector arrays, the corresponding result is simulated, and the pattern "H" is obtained (Fig. 5c). These results indicated that the pen-writing devices have a great potential for an image sensor.

4. Conclusion

We demonstrate a facile approach to prepare paper-based perovskite films and optoelectronic devices by pen-writing. It is found that the pen-writing seed layers can effectively promote the formation of planar-integrated single-crystal perovskite films with high quality on papers. With perovskite material and graphite as the photosensitive layer and the electrode, paper-

based perovskite photodetector arrays are written on papers. The photodetector presents a responsivity of 4.2 mA W^{-1} . Accordingly, the image sensor is fabricated with satisfied performance. This strategy provides an effective way to fabricate flexible and degradable optoelectronic devices.

Conflicts of interest

There are no conflicts to declare.

Acknowledgements

This work was supported financially by the National Key R&D Program of China (No. 2018YFA0208501), the National Natural Science Foundation of China (NSFC, No. 91963212, 52103236, 51773206, 21875260, 51961145102 and 62105293), K. C. Wong Education Foundation, Beijing National Laboratory for Molecular Sciences (No. BNLMS-CXXM-202005), the China Postdoctoral Science Foundation (No. 2021TQ0285), and Outstanding Young Talent Research Fund of Zhengzhou University. The authors also thank the Advanced Analysis & Computation Center at Zhengzhou University for materials and device characterization support.

References

- 1 H. Lu, W. Tian, B. Gu, Y. Zhu and L. Li, *Small*, 2017, **13**, 1701535.



2 J. Yang, C. Liu, C. Cai, X. Hu, Z. Huang, X. Duan, X. Meng, Z. Yuan, L. Tan and Y. Chen, *Adv. Energy Mater.*, 2019, **9**, 1900198.

3 S. S. H. Dintakurti, P. Vashishtha, D. Giovanni, Y. Fang, N. Foo, Z. Shen, C. Guet, T. C. Sum and T. White, *RSC Adv.*, 2021, **11**, 24137–24143.

4 Z. Huang, X. Hu, C. Liu, L. Tan and Y. Chen, *Adv. Funct. Mater.*, 2017, **27**, 1703061.

5 X. Jin, X. Zhang, H. Fang, W. Deng, X. Xu, J. Jie and X. Zhang, *Adv. Funct. Mater.*, 2018, **28**, 1705189.

6 X. Mo, T. Li, F. Huang, Z. Li, Y. Zhou, T. Lin, Y. Ouyang, X. Tao and C. Pan, *Nano Energy*, 2021, **81**, 105570.

7 Y. Yao, S.-W. Zhang, Z. Liu, C.-Y. Wang, P. Liu, L. Ma, G. Wei and F. Kang, *RSC Adv.*, 2021, **11**, 26415–26420.

8 W. Deng, L. Huang, X. Xu, X. Zhang, X. Jin, S. T. Lee and J. Jie, *Nano Lett.*, 2017, **17**, 2482–2489.

9 M. Wang, H. Sun, F. Cao, W. Tian and L. Li, *Adv. Mater.*, 2021, **33**, 2100625.

10 Y. Li, Z.-F. Shi, S. Li, L.-Z. Lei, H.-F. Ji, D. Wu, T.-T. Xu, Y.-T. Tian and X.-J. Li, *J. Mater. Chem. C*, 2017, **5**, 8355–8360.

11 Z. Yang, J. Lu, M. ZhuGe, Y. Cheng, J. Hu, F. Li, S. Qiao, Y. Zhang, G. Hu, Q. Yang, D. Peng, K. Liu and C. Pan, *Adv. Mater.*, 2019, **31**, 1900647.

12 L. N. Quan, B. P. Rand, R. H. Friend, S. G. Mhaisalkar, T. W. Lee and E. H. Sargent, *Chem. Rev.*, 2019, **119**, 7444–7477.

13 S. T. Han, H. Peng, Q. Sun, S. Venkatesh, K. S. Chung, S. C. Lau, Y. Zhou and V. A. L. Roy, *Adv. Mater.*, 2017, **29**, 1700375.

14 Y. S. Rim, S. H. Bae, H. Chen, N. De Marco and Y. Yang, *Adv. Mater.*, 2016, **28**, 4415–4440.

15 Y. Wang, Y. Liu, S. Cao and J. Wang, *J. Mater. Chem. C*, 2021, **9**, 5302–5322.

16 D. Hao, J. Zou and J. Huang, *InfoMat*, 2019, **2**, 139–169.

17 J. Jiang, S. Wang, X. Jia, X. Fang, S. Zhang, J. Zhang, W. Liu, J. Ding and N. Yuan, *RSC Adv.*, 2018, **8**, 12823–12831.

18 D. Yang, R. Yang, S. Priya and S. F. Liu, *Angew. Chem., Int. Ed.*, 2019, **58**, 4466–4483.

19 P. Zeng, W. Deng and M. Liu, *Sol. RRL*, 2020, **4**, 1900485.

20 T. Zhang, F. Wang, P. Zhang, Y. Wang, H. Chen, J. Li, J. Wu, L. Chen, Z. D. Chen and S. Li, *Nanoscale*, 2019, **11**, 2871–2877.

21 M. Wang, F. Cao, L. Meng, W. Tian and L. Li, *Adv. Mater. Interfaces*, 2019, **6**, 1801526.

22 Y. Xu, G. Zhao, L. Zhu, Q. Fei, Z. Zhang, Z. Chen, F. An, Y. Chen, Y. Ling, P. Guo, S. Ding, G. Huang, P. Y. Chen, Q. Cao and Z. Yan, *Proc. Natl. Acad. Sci. U. S. A.*, 2020, **117**, 18292–18301.

23 H. Liu, H. Jiang, F. Du, D. Zhang, Z. Li and H. Zhou, *ACS Sustainable Chem. Eng.*, 2017, **5**, 10538–10543.

24 F. Brunetti, A. Operamolla, S. Castro-Hermosa, G. Lucarelli, V. Manca, G. M. Farinola and T. M. Brown, *Adv. Funct. Mater.*, 2019, **29**, 1806798.

25 W. Wang, G. Li, Z. Jiang, Y. Zhang, T. Hu, J. Yi and Z. Chu, *Opt. Mater.*, 2021, **114**, 110926.

26 W. Deng, H. Huang, H. Jin, W. Li, X. Chu, D. Xiong, W. Yan, F. Chun, M. Xie, C. Luo, L. Jin, C. Liu, H. Zhang, W. Deng and W. Yang, *Adv. Opt. Mater.*, 2019, **7**, 1801521.

27 H. S. Jung, G. S. Han, N.-G. Park and M. J. Ko, *Joule*, 2019, **3**, 1850–1880.

28 H. Li, X. Li, W. Wang, J. Huang, J. Li, Y. Lu, J. Chang, J. Fang and W. Song, *Sol. RRL*, 2019, **3**, 1800317.

29 S. Cai, X. Xu, W. Yang, J. Chen and X. Fang, *Adv. Mater.*, 2019, **31**, 1808138.

30 M. I. Saidaminov, V. Adinolfi, R. Comin, A. L. Abdelhady, W. Peng, I. Dursun, M. Yuan, S. Hoogland, E. H. Sargent and O. M. Bakr, *Nat. Commun.*, 2015, **6**, 8724.

31 V. Adinolfi, O. Ouellette, M. I. Saidaminov, G. Walters, A. L. Abdelhady, O. M. Bakr and E. H. Sargent, *Adv. Mater.*, 2016, **28**, 7264.

32 Z. Gu, K. Wang, H. Li, M. Gao, L. Li, M. Kuang, Y. S. Zhao, M. Li and Y. Song, *Small*, 2017, **13**, 1603217.

33 Z. Gu, Z. Huang, X. Hu, Y. Wang, L. Li, M. Li and Y. Song, *ACS Appl. Mater. Interfaces*, 2020, **12**, 22157–22162.

34 H. Liu, X. Wei, Z. Zhang, X. Lei, W. Xu, L. Luo, H. Zeng, R. Lu and J. Liu, *J. Phys. Chem. Lett.*, 2019, **10**, 786–792.

35 M. I. Saidaminov, A. L. Abdelhady, B. Murali, E. Alarousu, V. M. Burlakov, W. Peng, I. Dursun, L. Wang, Y. He, G. Maculan, A. Goriely, T. Wu, O. F. Mohammed and O. M. Bakr, *Nat. Commun.*, 2015, **6**, 7586.

36 S. A. Hong-Hua Fang, H. Wei, J. Yang, G. R. Blake, J. Huang, J. Even and M. A. Loi, *Sci. Adv.*, 2016, **2**, 1600534.

37 X. Hu, X. Zhang, L. Liang, J. Bao, S. Li, W. Yang and Y. Xie, *Adv. Funct. Mater.*, 2014, **24**, 7373–7380.

38 S. X. Li, X. L. Xu, Y. Yang, Y. S. Xu, Y. Xu and H. Xia, *ACS Appl. Mater. Interfaces*, 2021, **13**, 31919–31927.

39 S. H. Cho, D. Kim and S.-M. Park, *Electrochim. Acta*, 2008, **53**, 3820–3827.

